Optimal Tracking Control of Current Profile in Tokamaks

Y. Ou, C. Xu, E. Schuster, T. C. Luce, J. R. Ferron, M. L. Walker, and D. A. Humphreys

***Abstract*—Setting up a suitable current spatial profile in tokamak plasmas has been demonstrated to be a key condition for one possible advanced scenario with improved confinement and possible steady-state operation. Experiments at the DIII-D tokamak focus on creating the desired current profile during the plasma current ramp-up and early flattop phases with the aim of maintaining this target profile during the subsequent phases of the discharge. The evolution in time of the current profile is related to the evolution of the poloidal magnetic flux, which is modeled in normalized cylindrical coordinates using a parabolic partial differential equation usually referred to as the magnetic diffusion equation. We propose a framework to solve a finite-time, optimal tracking control problem for the current profile evolution via diffusivity, interior, and boundary actuation during the ramp-up and early flattop phases of the discharge. The proposed approach is based on reduced order modeling via proper orthogonal decomposition and successive optimal control computation for a bilinear system. Simulation results illustrate the performance of the proposed controller.**

***Index Terms*—Bilinear optimal tracking control, distributed parameter systems, proper orthogonal decomposition (POD), tokamak plasma control.**

I. Introduction

NUCLEAR fusion is the process by which two nuclei stick together to form a heavier nucleus. This process is accompanied by a release of energy E, which is the result of the amount Δm of mass "lost" in the reaction. To make a fusion reaction possible, a certain amount of energy is required to bring the two repellant nuclei carrying positive charges sufficiently close. To overcome the Coulomb barrier, the kinetic energy of the nuclei is increased by heating. The temperature required for a thermonuclear fusion reaction to take place is around 100 million degrees. At much lower temperatures (about 10 thousand degrees), the electrons and nuclei separate and create an ionized gas called plasma, and also known as the fourth state of matter.

An intangible doughnut-shaped bottle created by magnetic lines is used to confine the high-temperature plasma. This type of magnetic confinement device is called Tokamak, an acronym for the Russian words Toroidalnaya Kamera ee Magnitnaya Katushka (toroidal chamber with magnetic coils), which was invented in the Soviet Union in the late 1950s [1]. A toroidal magnetic field is produced by the so-called "toroidal field" (TF) coils. The addition of a poloidal magneticc field (necessary for the existence of a magnetohydrodynamic (MHD) equilibrium [2]), generated by the toroidal plasma electric current and the "poloidal field" (PF) coils, produces a combined field in which the magnetic field lines twist their way around the tokamak to form a helical structure (see Fig. 1). It is possible to use the poloidal component $B_{\rm pol}$ of the helicoidal magnetic lines to define nested toroidal surfaces corresponding to constant values of the poloidal magnetic flux. The poloidal magnetic flux ψ at a point P is the total flux through the surface S bounded by the toroidal ring passing through P, i.e., $\psi = \int B_{\rm pol} dS$.

In a tokamak, the achievement of a suitable (toroidal) current profile plays an important role in enabling high fusion gain and noninductive sustainment of the plasma current for steady-state operation (see, e.g., [3]–[5]). The evolution in time of the current profile is related to the evolution of the poloidal magnetic flux, which is modeled in normalized cylindrical coordinates using a parabolic partial differential equation (PDE) usually referred to as the magnetic diffusion equation. The dynamics of the plasma current profile evolution can be modified by three actuators: the total plasma current, the non-inductive power, and the average plasma density. These actuators enter the magnetic

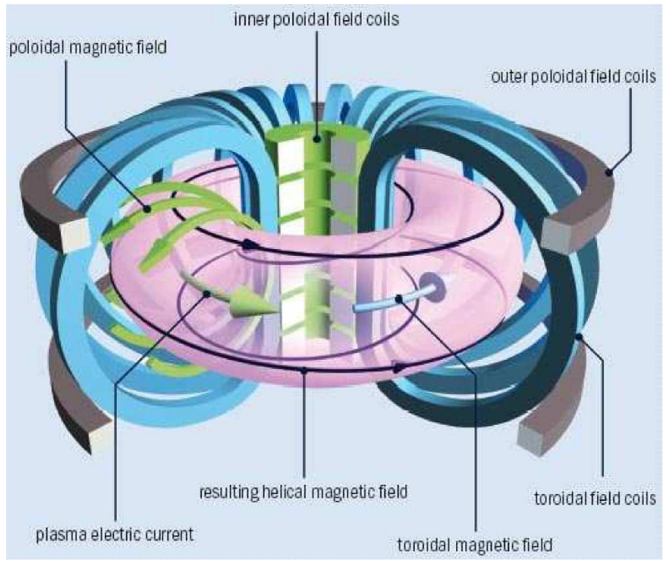

Fig. 1. Scheme of a tokamak device. The toroidal field (TF) coils are wrapped "poloidally" around the torus (the short way, going through the center hole), while the poloidal field (PF) coils are wrapped "toroidally" (the long way) around the torus. Current flowing in these conducting coils and in the plasma produces the helical magnetic field that confines the plasma (Source: ITER).

Manuscript received November 12, 2009; accepted January 17, 2010. Manuscript received in final form March 20, 2010. First published April 22, 2010; current version published February 23, 2011. Recommended by Associate Editor M. Mattei. This work was supported by the NSF CAREER Award Program (ECCS-0645086), and DoE Contract DE-FC02-04ER54698.

Y. Ou is with the Department of Mechanical Engineering and Mechanics, Lehigh University, Bethlehem, PA 18015 USA and also with the Shenzhen Institutes of Advanced Technology, Chinese Academy of Science, Guangdong 518055, China (e-mail: yoo205@lehigh.edu).

C. Xu and E. Schuster are with the Department of Mechanical Engineering and Mechanics, Lehigh University, Bethlehem, PA 18015 USA.

T. C. Luce, J. R. Ferron, M. L. Walker, and D. A. Humphreys are with the DIII-D tokamak, General Atomics, San Diego, CA 92121 USA.

Color versions of one or more of the figures in this paper are available online at http://ieeexplore.ieee.org.

Digital Object Identifier 10.1109/TCST.2010.2046640

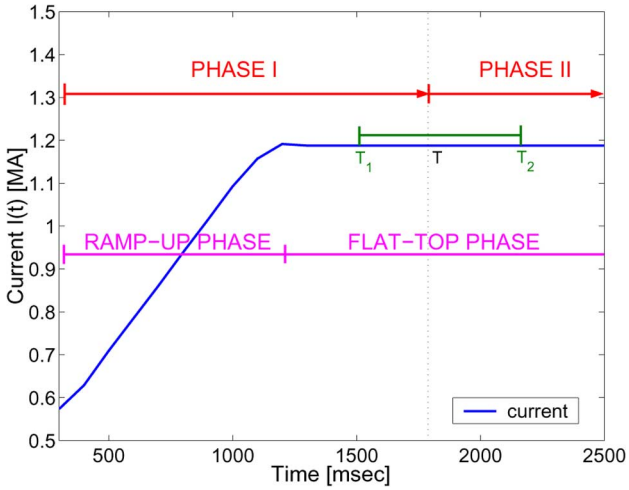

Fig. 2. Current evolution defines the phases of the tokamak discharge.

diffusion equation as interior, boundary, and diffusivity control terms.

One possible approach to current profile control is to focus on creating the desired current profile during the plasma current ramp-up and early flattop phases of the tokamak discharge with the aim of maintaining this target profile during the subsequent phases of the discharge. Since the actuators that are used to achieve the desired target profile are constrained, experiments have shown that some of the desirable target profiles may not be achieved for all arbitrary initial condition. Therefore, a perfect matching of the desirable target profile may not be physically possible. In practice, the objective is to achieve the best possible approximate matching at final time $t_f = T$ during the early flattop phase of the total plasma current pulse, as shown in Fig. 2. Thus, such matching problem can be formulated as a finite-time optimal control problem for the magnetic diffusion PDE.

Our current work includes the investigation of the use extremum seeking [6] and nonlinear programming [7] to achieve an open-loop control solution for this optimal problem. The work is aimed at saving long trial-and-error periods of time currently spent by fusion experimentalists trying to manually adjust the time evolutions of the actuators to achieve the desired current profile at some prespecified time. However, the reproduction of the nominal initial conditions is usually challenging and sometimes impossible for the operators, who can only guarantee that the real initial conditions are within a neighborhood of the nominal ones. Therefore, in this work we propose a closed-loop optimal control law aimed at rejecting disturbances in initial conditions. The objective of the closed-loop (feedback) optimal controller is to track the undisturbed open-loop (feedforward) system trajectory.

Optimal feedback control design for PDE systems is very challenging and usually unfeasible due to the infinite dimensionality of the problem. In this paper, we use proper orthogonal decomposition (POD) and Galerkin methods to obtain a low dimensional dynamical model for the PDE system. The POD method is an efficient approach to obtain low-dimensional dynamical models from data ensembles arising from numerical simulation or experimental observation. By using POD it is possible to extract the dominant low-dimensional dynamics from the infinite dimensional dynamical system. The method has been widely and successfully used, particulary in the area of fluid dynamics (e.g., [8]). Fundamental aspects of the POD method applied to parabolic problems, such as error estimates for POD-Galerkin model reduction applied to both linear and nonlinear systems, are discussed in [9].

Due to the presence of the diffusivity control term in the magnetic diffusion equation, the low dimensional dynamical model obtained turns to be bilinear. To track the open loop control trajectory for any initial condition, minimize the control effort, and match a target profile as closely as possible at a prespecified time $t_f = T$, a closed-loop finite-time optimal tracking control problem for a finite-dimensional bilinear system must be solved. Inspired by [10], the two-point-boundary-value (TPBV) problem arising from the optimality conditions for the bilinear system is solved using a convergent scheme based on an iterative quasi-linear approximation approach. Convergence of the iterative scheme is proved in appropriate functional spaces by using the contraction mapping theorem.

This paper is organized as follows. In Section II, an infinite-dimensional dynamic model for the poloidal flux ψ is introduced. Section III describes the control objectives during the different phases of the tokamak discharge, and states the control problem. In Section IV, we discuss the POD method as well as the Galerkin projection method based on a test function set composed by dominant POD modes. After obtaining a low dimensional bilinear system, in Section V, we derive the optimality conditions and propose an iterative convergent scheme, based on the quasi-linear approximation of the system dynamics, to solve the optimal control problem. A simulation study showing the effectiveness of the proposed feedback controller is presented in Section VI. Conclusions and future work are presented in Section VII.

II. Current Profile Evolution Model

We let ρ be an arbitrary coordinate indexing the magnetic surfaces. Any quantity constant on each magnetic surface could be chosen as the variable ρ. We choose the mean geometric radius of the magnetic surface as the variable ρ, i.e., $\pi B_{\phi,o}\rho^2 = \Phi$, where Φ is the toroidal magnetic flux and $B_{\phi,o}$ is the reference toroidal magnetic field at the geometric plasma center R_o. The variable $\hat{\rho}$ denotes the normalized radius (ρ/ρ_b), and ρ_b is the radius of the last closed flux surface. The evolution of the poloidal flux in normalized cylindrical coordinates is given by the magnetic diffusion equation [4]

$$\frac{\partial \psi}{\partial t} = \frac{\eta(T_e)}{\mu_o \rho_b^2 \hat{F}^2 \hat{\rho}} \frac{\partial}{\partial \hat{\rho}} \left(\hat{\rho} \hat{F} \hat{G} \hat{H} \frac{\partial \psi}{\partial \hat{\rho}} \right) - R_o \hat{H} \eta(T_e) \frac{\langle \bar{j}_{NI} \cdot \bar{B} \rangle}{B_{\phi,o}} \tag{1}$$

where t is the time, ψ is the poloidal magnetic flux, η is the plasma resistivity, T_e is the plasma electron temperature, μ_o is the vacuum permeability, $\bar{j}_{NI}$ is the non-inductive source of current density (neutral beam, electron cyclotron, etc.), $\bar{B}$ is the toroidal magnetic field, and $\langle\rangle$ denotes flux-surface average. $\hat{F}$, $\hat{G}$, $\hat{H}$ are geometric factors, which are functions of $\hat{\rho}$ and are given in [6]. The boundary conditions are given by

$$\left.\frac{\partial \psi}{\partial \hat{\rho}}\right|_{\hat{\rho}=0} = 0, \quad \left.\frac{\partial \psi}{\partial \hat{\rho}}\right|_{\hat{\rho}=1} = \frac{\mu_o}{2\pi} \frac{R_o}{\hat{G}\Big|_{\hat{\rho}=1} \hat{H}\Big|_{\hat{\rho}=1}} I(t) \tag{2}$$

where $I(t)$ denotes the total plasma current.

The model makes the simplifying assumption that the magnetic geometry is fixed in time. This excludes two potential sources of flux—a change in ρ_b (either by a change in the shape of the last closed flux surface or in $B_{\phi,o}$) and a change in location of the geometric center of the interior flux surfaces relative to that of the last closed flux surface. It is straightforward to include the effect of a change in ρ_b in the model for situations where it would be important. However, we focus in this work on the design of a current profile controller to be activated during the late stage of the ramp-up phase, where the plasma shape has already developed and is approximately fixed, which implies that changes in ρ_b are small by design in the experiments of interest ($B_{\phi,o}$ is also approximately constant). Changes in the relative positions of the flux surfaces do occur, but for cases of interest, these happen slowly enough and they can be neglected.

During "Phase I" (see Fig. 2), mainly governed by the ramp-up phase, the plasma current is mostly driven by induction. In this case, it is possible to decouple the equation for the evolution of the poloidal flux from the evolution equation for the temperature $T_e(\hat{\rho},t)$. Simplified scenario-oriented models for the temperature and non-inductive toroidal current density are chosen for this phase. Based on experimental observations at DIII-D, the shapes of the profiles are assumed to remain fixed and equal to the so-called reference profiles, which are identified from DIII-D discharges associated with the experiment of interest [4]. The responses to the actuators are simply scalar multiples of the reference profiles. The temperature T_e is assumed to follow $\left(I(t)\sqrt{P_{\rm tot}}/\bar{n}(t)\right)$, and can be written as $T_e(\hat{\rho},t) = k_{Te}T_e^{\rm profile}(\hat{\rho}) \quad \left(I(t)\sqrt{P_{\rm tot}}/\bar{n}(t)\right)$, where the reference profile $T_e^{\rm profile}(\hat{\rho})$ is only function of the space coordinate [6], $k_{Te} = 1.7295 \cdot 10^{10}$ ($\mathrm{m^{-3}A^{-1}W^{-1/2}}$), $P_{\rm tot}$ is the total power of the non-inductive current sources [electron cyclotron heating (ECH), neutral beam heating (NBH), etc.], and $\bar{n}$ is the line-averaged plasma density. The non-inductive toroidal current density $(\langle \vec{j}_{NI} \cdot \vec{B} \rangle / B_{\phi,o})$ is assumed to follow $(\langle \vec{j}_{NI} \cdot \vec{B} \rangle / B_{\phi,o}) = k_{NIpar} j_{NIpar}^{\rm profile}(\hat{\rho}) \left(I(t)^{1/2}P_{\rm tot}(t)^{5/4}/\bar{n}(t)^{3/2}\right)$, where the reference profile $j_{NIpar}^{\rm profile}$ is only function of the space coordinate [6], and $k_{NIpar} = 1.2139 \cdot 10^{18}$ ($\mathrm{m^{-9/2}A^{-1/2}W^{-5/4}}$). The resistivity η scales with the temperature T_e as $\eta(\hat{\rho},t) = \left(k_{\rm eff}Z_{\rm eff}/T_e^{3/2}(\hat{\rho},t)\right)$, where $Z_{\rm eff} = 1.5$, and $k_{\rm eff} = 4.2702 \cdot 10^{-8}$ ($\Omega\mathrm{m(kev)}^{3/2}$). The proposed time scaling in terms of $I(t)$, $P_{\rm tot}(t)$, and $\bar{n}(t)$ has been successfully validated in experiments [6]. Since this is a scenario-oriented model, the accuracy of the predicted profile shapes for the temperature and non-inductive toroidal current density depends however on how well the discharge conditions present at the moment of identifying the reference profiles are reproduced.

We consider $\bar{n}(t)$, $I(t)$, and $P_{\rm tot}(t)$ as the actuators of the system. However, the waveforms for $\bar{n}(t), I(t)$, and $P_{\rm tot}(t)$ generated by the controller proposed in this work indeed represent the desired values for these controlled variables and therefore the references to dedicated controllers. For instance, in the case of the plasma current, a proportional-integral-differential (PID) loop usually regulates the ohmic coil voltage to make the plasma current measured by a Rogowski loop (which includes both inductive and non-inductive current components) follow the desired waveform generated by the controller. Similarly to the case of the plasma current, a PID loop regulates gas puffing and pumping to make the line averaged density measured by a CO_2 interferometer follow the desired waveform. The power of the current drives is directly controlled by the power supplies associated with the drives.

III. Control Problem Description

During "Phase I" the control goal is to drive the current profile from any arbitrary initial condition to a prescribed target or desirable profile at some time $T \in (T_1, T_2)$ (here $T_1 = 1.2s$ and $T_2 = 2.4s$) in the flat-top phase of the total current $I(t)$ evolution. During "Phase II" the control goal is to regulate the current profile around this target profile.

It is worth to note that we can rewrite the equation for the evolution of the poloidal flux (1) as

$$\frac{1}{f_1(\hat{\rho})}\frac{\partial \psi}{\partial t} = u_1(t)\frac{1}{\hat{\rho}}\frac{\partial}{\partial \hat{\rho}}\left(\hat{\rho}f_4(\hat{\rho})\frac{\partial \psi}{\partial \hat{\rho}}\right) + f_2(\hat{\rho})u_2(t)\frac{1}{f_1(\hat{\rho})} \tag{3}$$

with boundary conditions $(\partial\psi/\partial\hat{\rho})\big|_{\hat{\rho}=0} = 0$, $(\partial\psi/\partial\hat{\rho})\big|_{\hat{\rho}=1} = k_3u_3(t)$, where $k_3 = (\mu_o/2\pi)\left(R_o/\hat{G}\Big|_{\hat{\rho}=1}\hat{H}\Big|_{\hat{\rho}=1}\right)$, and where

$$\begin{aligned} f_1(\hat{\rho}) &= \frac{k_{\rm eff}Z_{\rm eff}}{k_{Te}^{3/2}\mu_o\rho_b^2}\frac{1}{\hat{F}^2(\hat{\rho})(T_e^{\rm profile}(\hat{\rho}))^{3/2}} \\ f_2(\hat{\rho}) &= -\frac{k_{\rm eff}Z_{\rm eff}R_ok_{NIpar}}{k_{Te}^{3/2}}\frac{\hat{H}(\hat{\rho})j_{NIpar}^{\rm profile}(\hat{\rho})}{(T_e^{\rm profile}(\hat{\rho}))^{3/2}} \\ f_4(\hat{\rho}) &= \hat{F}\hat{G}\hat{H} \end{aligned} \tag{4}$$

and

$$\begin{aligned} u_1(t) &= \left(\frac{\bar{n}(t)}{I(t)\sqrt{P_{\rm tot}}}\right)^{3/2} \\ u_2(t) &= \frac{\sqrt{P_{\rm tot}(t)}}{I(t)} \\ u_3(t) &= I(t). \end{aligned} \tag{5}$$

The control of the magnetic diffusion PDE (3) is unique in the sense that it admits control not only through $u_2(t)$ (interior control) and $u_3(t)$ (boundary control) but also through $u_1(t)$, what we name *diffusivity control* in this paper.

In practice, the toroidal current density is usually specified indirectly by the rotational transform ι (or the safety factor $q = \iota^{-1}$), which is defined as $\iota(\rho,t) = (\partial\psi(\rho,t)/\partial\Phi)$. The constant relationship between Φ and ρ, $\rho = \sqrt{(\Phi/\pi B_{\phi,o})}$, and the definition of the normalized radius $\hat{\rho}$ allow us to rewrite the rotational transform as $\iota(\hat{\rho},t) = (\partial\psi/\partial\hat{\rho})(1/B_{\phi,o}\rho_b^2\hat{\rho})$. Since ι is uniquely defined by the spatial derivative of the magnetic flux ψ, in this work we define the to-be-controlled variable as

$$\theta(\hat{\rho},t) = \frac{\partial\psi}{\partial\hat{\rho}} \tag{6}$$

and use (3) to obtain a PDE for $\theta(\hat{\rho},t)$. To simplify notation, we replace $\hat{\rho}$ by x hereafter. The control objective is to drive $\theta(x,t)$ from any arbitrary initial profile $\theta_{\rm ini}(x)$ to a prescribed target or

desirable profile $\theta^{\text{des}}(x)$ at some time $t_f = T$. Using (6) we can rewrite (3) as

$$\frac{\partial \psi}{\partial t} = g_1(x)u_1(t)\left(g_2(x)\theta(x,t)\right)' + g_3(x)u_2(t) \tag{7}$$

with $g_1(x) = f_1(x)(1/x)$, $g_2(x) = xf_4(x)$, $g_3(x) = f_2(x)$, where "f'" stands for derivative of f w.r.t. x, i.e., $f' = (\partial f/\partial x)$. By differentiating both sides of (7) w.r.t. x, and letting $h_0(x) = g_1(x)g_2(x)$, $h_1(x) = g_1'(x)g_2(x) + 2g_1(x)g_2'(x)$, $h_2(x) = g_1'(x)g_2'(x) + g_1(x)g_2''(x)$, $h_3(x) = g_3'(x)$, we can finally write

$$\begin{aligned}\frac{\partial \theta(x,t)}{\partial t} &= h_0(x)\theta''(x,t)u_1(t) + h_1(x)\theta'(x,t)u_1(t) \\ &\quad + h_2(x)\theta(x,t)u_1(t) + h_3(x)u_2(t)\end{aligned} \tag{8}$$

with boundary conditions $\theta(0,t) = 0$, $\theta(1,t) = k_3u_3(t)$, and initial condition $\theta(x,0) = \theta_{\text{ini}}(x)$.

IV. Model Reduction Using POD/Galerkin

A. POD Modes

The set $\mathcal{V} = \text{span}\{\theta_1, \ldots, \theta_n\} \subset \mathbb{R}^m$ refers to a data ensemble consisting of snapshots $\{\theta_j\}_{j=1}^n$ obtained from simulation or experimental observation on the grid $\mathcal{Q}_{ij} = (x_i, t_j)$, where i, j are integers with $1 \le i \le m$; $1 \le j \le n$ ($\theta_j(i) = \theta(x_i, t_j)$). Let $\{\varphi_k\}_{k=1}^d$ be an orthonormal basis of the data ensemble $\mathcal{V}$, where $d = \dim \mathcal{V} \le m$. We then project each of the snapshots onto the basis φ_k

$$\theta_j = \sum_{k=1}^{d} (\theta_j, \varphi_k)\varphi_k, \quad j = 1, \ldots, n \tag{9}$$

where $(\cdot,\cdot)$ denotes the vector inner product. The goal of the POD method is to find an orthonormal basis such that for some predefined $1 \le l \le d$ the following average index is minimized:

$$\begin{aligned}\min_{\{\varphi_k\}_{k=1}^l} \quad & \frac{1}{n}\sum_{j=1}^{n}\left\|\theta_j - \sum_{k=1}^{l}(\theta_j, \varphi_k)\varphi_k\right\|^2 \\ \text{subject to} \quad & (\varphi_i, \varphi_j) = \delta_{ij}, \quad 1 \le i \le l, \ 1 \le j \le i\end{aligned} \tag{10}$$

where $\|\theta\| = \sqrt{(\theta,\theta)} = \sqrt{\theta^T\theta}$ and δ_{ij} denotes the Kronecker delta, which is one when $i = j$ and zero otherwise.

The solution of (10) can be found in the literature, e.g., [8], [9]. Defining the correlation matrix $K \in \mathbb{R}^{n\times n}$ as $K_{ij} = (1/n)(\theta_j, \theta_i)$, for $i, j = 1, \ldots, n$, let $\Lambda_1 > \cdots > \Lambda_l > \cdots > \Lambda_d > 0$ denote the positive eigenvalues of the correlation matrix K and $\chi_1, \ldots, \chi_l, \ldots, \chi_d$ the associated eigenvectors, where $d = \text{rank}(K)$. Then, the POD basis functions take the form

$$\varphi_k = \frac{1}{\sqrt{\Lambda_k}}\sum_{j=1}^{n}(\chi_k)_j\theta_j = \frac{1}{\sqrt{\Lambda_k}}\Theta\chi_k, \quad (k = 1, \ldots, d) \tag{11}$$

where $(\chi_k)_j$ is the jth component of the eigenvector χ_k and $\Theta = (\theta_1, \ldots, \theta_n)$ is the collection of all the snapshots. Moreover, the error (energy ratio) associated with the approximation with the first l POD modes is

$$\varepsilon_l = \frac{1}{n}\sum_{j=1}^{n}\left\|\theta_j - \sum_{k=1}^{l}(\theta_j^T\varphi_k)\varphi_k\right\|^2 = \sum_{k=l+1}^{d}\Lambda_k. \tag{12}$$

B. Galerkin Projection

Let $V_{\text{POD}} = \{\varphi_1, \varphi_2, \varphi_3, \varphi_4, \ldots, \varphi_l\}$ be the set of obtained POD modes. Using the l POD modes, we approximate the system state as $\theta(x,t) \approx \theta^l(x,t) = \sum_{i=1}^{l}\alpha_i(t)\phi_i(x)$, where continuous POD basis functions $\phi_i(x) \in L^2([0,1])$ are obtained by interpolating the POD modes φ_i (vectors). We substitute this expression in (8) to obtain

$$\begin{aligned}&\sum_{i=1}^{l}\dot{\alpha}_i(t)\phi_i(x) \\ &\quad = h_0(x)u_1(t)\sum_{i=1}^{l}\alpha_i(t)\frac{\partial^2\phi_i}{\partial x^2} + h_1(x)u_1(t)\sum_{i=1}^{l}\alpha_i(t)\frac{\partial\phi_i}{\partial x} \\ &\qquad + h_2(x)u_1(t)\sum_{i=1}^{l}\alpha_i(t)\phi_i(x) + h_3(x)u_2(t).\end{aligned} \tag{13}$$

In order to write the *weak form* of (13) we define first

$$\begin{aligned}\langle g_1 g_2 \cdots g_n\rangle &\triangleq \int_0^1 g_1 g_2 \ldots g_n dx \\ &\approx \sum_{n=1}^{N} g_1(n\Delta x)g_2(n\Delta x)\ldots g_n(n\Delta x) \\ &\triangleq \ll g_1 g_2 \ldots g_n \gg^N\end{aligned} \tag{14}$$

where Δx is the spatial interval size and $N+1$ is the number of grid points ($N\Delta x = 1$) considered for the numerical approximation of the interior product. The grid $\vec{x} = [0 \ \ \Delta x \ \ 2\Delta x \ \ \ldots \ \ (N-1)\Delta x \ \ 1]^T$, is partitioned as $\vec{x} = [[0 \ \ \Delta x \ \ 2\Delta x \ \ \ldots \ \ (N-1)\Delta x]^T \ \ 1]^T \triangleq [\vec{x}_o^T \ \ 1]^T$. We then multiply both sides of (13) by $\phi_k(x)$, for $k = 1, 2, \ldots, l$, integrate over the spatial domain $[0,1]$, and take into account that the POD basis functions $\phi_i(x)$ are orthonormal, i.e., $\langle\phi_i(x), \phi_j(x)\rangle = \delta_{ij}$, to obtain

$$\begin{aligned}&\dot{\alpha}_k(t) \\ &= u_2(t) \ll h_3, \phi_k \gg^N \\ &\quad + u_1(t)\sum_{i=1}^{l}\alpha_i(t)\left[\ll h_0, \phi_i'', \phi_k \gg^{N-1} + h_0(1)\phi_i''(1)\phi_k(1)\right] \\ &\quad + u_1(t)\sum_{i=1}^{l}\alpha_i(t)\left[\ll h_1, \phi_i', \phi_k \gg^{N-1} + h_1(1)\phi_i'(1)\phi_k(1)\right] \\ &\quad + u_1(t)\sum_{i=1}^{l}\alpha_i(t)[\ll h_2, \phi_i, \phi_k \gg^{N-1} + h_2(1)\phi_i(1)\phi_k(1)].\end{aligned} \tag{15}$$

C. Inclusion of Boundary Control in Reduced-Order Model

Dirichlet boundary control cannot be effectively incorporated into the reduced-order model by following a conventional integration-by-parts approach during the Galerkin projection. Specific difficulties in Dirichlet boundary control problems result from the fact that they are not of variational type [11], [12]. Inspired by [13], we overcome this problem by using a spatial discretization (14) of the interior product during the Galerkin projection and employing the end-point-separation method as shown below. We rewrite the boundary condition as

$$\theta|_{x=1} = \sum_{i=1}^{l} \alpha_i(t)\phi_i(1) = k_3 u_3(t). \tag{16}$$

From (16) we can write

$$\alpha_k(t)\phi_k(1) = k_3 u_3(t) - \sum_{i=1}^{l}(1-\delta_{i,k})\alpha_i(t)\phi_i(1). \tag{17}$$

By using (17) we can obtain

$$\begin{aligned} &u_1(t)h_0(1)\sum_{i=1}^{l}\alpha_i(t)\phi_k(1)\phi_i''(1) \\ &\quad = u_1(t)h_0(1)\alpha_k(t)\phi_k(1)\phi_k''(1) \\ &\qquad + u_1(t)h_0(1)\sum_{i=1}^{l}(1-\delta_{i,k})\alpha_i(t)\phi_k(1)\phi_i''(1) \\ &\quad = u_1(t)h_0(1)k_3u_3(t)\phi_k''(1) \\ &\qquad + u_1(t)h_0(1)\sum_{i=1}^{l}\alpha_i(t)\left[\phi_k(1)\phi_i''(1) - \phi_i(1)\phi_k''(1)\right]. \end{aligned} \tag{18}$$

We follow similar procedure to write

$$\begin{aligned} u_1(t)h_1(1)\sum_{i=1}^{l}\alpha_i(t)\phi_k(1)\phi_i'(1) &= u_1(t)h_1(1)k_3u_3(t)\phi_k'(1) \\ +u_1(t)h_1(1)\sum_{i=1}^{l}\alpha_i(t)&(\phi_k(1)\phi_i'(1) - \phi_i(1)\phi_k'(1)) \end{aligned} \tag{19}$$

and

$$u_1(t)h_2(1)\sum_{i=1}^{l}\alpha_i(t)\phi_k(1)\phi_i(1) = u_1(t)h_2(1)k_3u_3(t)\phi_k(1). \tag{20}$$

By substituting (18)–(20) into (15), using the notation

$$\begin{aligned} \Gamma_{ki} &= \ll h_0, \phi_i'', \phi_k \gg^N - h_0(1)\phi_i(1)\phi_k''(1) \\ &\quad + \ll h_1, \phi_i', \phi_k \gg^N - h_1(1)\phi_i(1)\phi_k'(1) \\ &\quad + \ll h_2, \phi_i, \phi_k \gg^{N-1} \\ \Phi_k &= \ll h_3, \phi_k \gg^N \\ \Pi_k &= h_0(1)k_3\phi_k''(1) + h_1(1)k_3\phi_k'(1) + h_2(1)k_3\phi_k(1) \end{aligned}$$

and redefining the control vector as

$$u = (v_1, v_2, v_3)^T = (u_1, u_2, u_1u_3)^T \tag{21}$$

we obtain a matrix representation for the reduced order model

$$\frac{d\bar{\alpha}}{dt} = \Gamma\bar{\alpha}v_1(t) + \Phi v_2(t) + \Pi v_3(t) \tag{22}$$

where $\bar{\alpha}(t) = (\alpha_1, \ldots, \alpha_l)^T \in \mathbb{R}^l, \Gamma \in \mathbb{R}^{l\times l}, \Phi, \Pi \in \mathbb{R}^{l\times 1}$, and $v_i \in \mathbb{R}^1$, for $i = 1, 2, 3$. The vector $\bar{\alpha}(t)$ is the finite dimensional approximation of $\theta(x,t)$, w.r.t. the associated POD modes.

V. Optimal Tracking Control Design

A. Optimal Control Problem Statement

We let $v^o(t) = [\,v_1^o \quad v_2^o \quad v_3^o\,]^T$ be a set of open-loop control trajectories, which are computed offline, and $\alpha^o(t)$ be the open-loop state trajectory associated with the open-loop control $v^o(t)$, with a nominal initial state α_0^o. The open-loop state trajectory satisfies

$$\frac{d\alpha^o}{dt} = \Gamma\alpha^o v_1^o(t) + \Phi v_2^o(t) + \Pi v_3^o(t) \tag{23}$$

with initial condition $\alpha^o(t_0) = \alpha_0^o$. Let us define $e(t) = \alpha(t) - \alpha^o(t)$ and $v^c(t) = v(t) - v^o(t)$, where $v(t) = [\,v_1 \quad v_2 \quad v_3\,]^T$ is the overall control input and $v^c(t) = [\,v_1^c \quad v_2^c \quad v_3^c\,]^T$ is the to-be-designed closed-loop control, which is appended to the open-loop control $v^o(t)$. Then, we can write

$$\frac{d\alpha^o}{dt} + \frac{de}{dt} = \Gamma(\alpha^o + e)\,(v_1^o + v_1^c) + \Phi\,(v_2^o + v_2^c) + \Pi\,(v_3^o + v_3^c)\,. \tag{24}$$

By substituting (23) into (24), we obtain

$$\frac{de}{dt} = A(t)e + B(e)u = f(e,u) \tag{25}$$

where $A(t) = \Gamma v_1^o(t) \in \mathbb{R}^{l\times l}$, $B(e) = [\,\Gamma(e+\alpha^o) \quad \Phi \quad \Pi\,] \in \mathbb{R}^{l\times 3}$, $u(t) = v^c(t) = [\,v_1^c \quad v_2^c \quad v_3^c\,]^T \in \mathbb{R}^{3\times 1}$.

We state the optimal control problem for the reduced-order ODE system (25) as

$$\begin{aligned} \min_u J = \frac{1}{2}e^T(t_f)Se(t_f) + \frac{1}{2}\int_{t_0}^{t_f} e^T(t)\Omega(t)e(t)dt \\ + u^T(t)R(t)u(t)dt \end{aligned} \tag{26}$$

where S and Ω are symmetric positive semi-definite matrices and R is a symmetric positive definite matrix. By introducing the Lagrange multiplier $\lambda(t) \in \mathbb{R}^{l\times 1}$, we can define the Hamiltonian

$$\begin{aligned} H(e,u,\lambda) = \frac{1}{2}e^T(t)\Omega(t)e(t) + \frac{1}{2}u^T(t)R(t)u(t) \\ + \lambda^T(t)[A(t)e(t) + B(e)u(t)]. \end{aligned} \tag{27}$$

By invoking the principle of optimality, $(\partial H/\partial u) = 0$, we obtain

$$R(t)u(t) + B^T(e)\lambda(t) = 0.$$

Then, the optimal control law is given by

$$u^*(t) = -R^{-1}(t)B^T(e)\lambda(t). \tag{28}$$

The optimal solution is characterized by the following set of differential equations in the state e and costate λ

$$\begin{aligned}\dot{e} &= \frac{\partial H}{\partial \lambda} = A(t)e + B(e)u(t)\\ \dot{\lambda} &= -\frac{\partial H}{\partial e} = -\Omega(t)e - A(t)^T\lambda(t) - u^T(t)\frac{\partial B^T(e)}{\partial e}\lambda(t)\end{aligned} \tag{29}$$

which define a two-point-boundary-value (TPBV) problem with $e(t_0) = e_0 = x_0 - x_0^o$, $\lambda(t_f) = Se(t_f)$.

B. Solution by Quasi-Linear Approximation

The solution of the nonlinear TPBV problem is usually computationally demanding. In this section, we propose a successive approach based on a quasi-linear approximation of the system dynamics [10] to solve the TPBV problem. By expanding our problem (25) up to first-order around the previous iteration trajectories $e^k(t)$ and $u^k(t)$, the system (25) takes the form

$$\dot{e}^{k+1} = A(t)e^{k+1} + B^k(t)u^{k+1} \tag{30}$$

where k is the iteration number and

$$B^k(t) = B(e)|_{e=e^k(t)} \tag{31}$$

with initial condition $e^{k+1}(0) = e_0$. The cost function takes the form

$$\begin{aligned}J^{k+1} = &\frac{1}{2}\left(e^{k+1}(t_f)\right)^T Se^{k+1}(t_f)\\ &+ \frac{1}{2}\int_{t_0}^{t_f}(e^{k+1}(t))^T\Omega(t)e^{k+1}(t)\\ &+ (u^{k+1}(t))^T R(t)u^{k+1}(t)dt\end{aligned} \tag{32}$$

and the Hamilton is written as

$$\begin{aligned}&H(e^{k+1}, u^{k+1}, \lambda^{k+1})\\ &= \frac{1}{2}(e^{k+1}(t))^T\Omega(t)e^{k+1}(t)\\ &\quad + \frac{1}{2}(u^{k+1}(t))^T R(t)u^{k+1}(t)\\ &\quad + (\lambda^{k+1})^T(t)[A(t)e^{k+1}(t) + B^k(t)u^{k+1}(t)].\end{aligned} \tag{33}$$

For each iteration, we have a standard linear quadratic optimal control problem defined by (30) and (32) with the approximate control law given by

$$u^{k+1}(t) = -R^{-1}(t)(B^k)^T\lambda^{k+1}(t). \tag{34}$$

As explained above, the optimal problem is characterized by the following TPBV:

$$\begin{aligned}\dot{e}^{k+1} &= A(t)x^{k+1} + B^k(-R^{-1}(t)(B^k)^T\lambda^{k+1}(t))\\ \dot{\lambda}^{k+1} &= -\Omega(t)e^{k+1}(t) - A(t)^T\lambda^{k+1}(t)\end{aligned} \tag{35}$$

along with the boundary conditions

$$e^{k+1}(t_0) = e_0, \quad \lambda^{k+1}(t_f) = Se^{k+1}(t_f). \tag{36}$$

Let us propose the solution form

$$\lambda^{k+1}(t) \triangleq s^{k+1}(t)e^{k+1}(t) \tag{37}$$

where $s^{k+1}(t)$ is a $l \times l$ symmetric matrix. Substituting (37) into (35), we can obtain the following Riccati matrix differential equation

$$\dot{s}^{k+1} = -A^T s^{k+1} - s^{k+1}A - \Omega + s^{k+1}B^k R^{-1}(B^k)^T s^{k+1} \tag{38}$$

with terminal condition $s^{k+1}(t_f) = S$. Then, the closed-loop system becomes

$$\dot{e}^{k+1} = (A - B^k R^{-1}(B^k)^T s^{k+1})e^{k+1} \tag{39}$$

with the initial condition $e^{k+1}(t_0) = e_0$.

The open-loop state trajectories $x^o(t)$ are used to evaluate (31) and start the iterations. The iterative procedure is stopped when convergence is achieved under given error tolerance. Finally, by using the convergent solution $s(t)$ of the Riccati (38), we obtain the following feedback control law

$$u^*(t) = -R^{-1}(t)B^T(e)s^*(t)e(t). \tag{40}$$

The weight matrix R can be used to satisfy the magnitude constraints of the actuators.

Proof of Convergence for the Iterative Scheme

In the rest of this section, it remains to prove the convergence of the proposed quasi-linear approximation in solving the optimal control problem. Namely, we will show the following limits in appropriate functional spaces

$$\lim_{k\to\infty} \mathrm{e}^{(k)} = \mathrm{e}^*, \quad \lim_{k\to\infty} s^{(k)} = s^*. \tag{41}$$

The associated spaces are two Banach spaces , $\mathfrak{B}_1 = C([t_0, t_f], \mathbb{R}^l)$, $\mathfrak{B}_2 = C([t_0, t_f], \mathbb{R}^{l\times l})$, with norms $\|\mathrm{e}\|_{\mathfrak{B}_1} = \sup_{\tau\in[t_0,t_f]}\|\mathrm{e}(\tau)\|$, for any $\mathrm{e} \in \mathfrak{B}_1$ and $\|s\|_{\mathfrak{B}_2} = \sup_{\tau\in[t_0,t_f]}\|s(\tau)\|$, for any $s \in \mathfrak{B}_2$, where $\|\mathrm{e}\| = \sqrt{\sum_{i=1}^l \mathrm{e}_i^2}$, and $\|s\| = \sqrt{\sum_{i=1}^l s_i^2}$.

Remark 1: To show (41), we only need to show that both $\{\mathrm{e}^{(k)}\}$ and $\{s^{(k)}\}$ are Cauchy sequences. Thus, the convergence follows due to the completeness of the Banach spaces. The convergence proof is based on the contraction mapping theorem for Banach spaces, which is motivated by the convergence proof in [10].

Based on (38) and (39), we obtain differential equations for the differences $\mathrm{e}^{(k+1)} - \mathrm{e}^{(k)}$ and $s^{(k+1)} - s^{(k)}$

$$\begin{aligned}&\frac{d}{dt}\left[\mathrm{e}^{(k+1)} - \mathrm{e}^{(k)}\right]\\ &\quad = \mathfrak{A}^{(k)}\left(\mathrm{e}^{(k+1)} - \mathrm{e}^{(k)}\right) + \left(\mathfrak{A}^{(k)} - \mathfrak{A}^{(k-1)}\right)\mathrm{e}^{(k)}\end{aligned} \tag{42}$$

$$\begin{aligned}&\frac{d}{dt}\left[s^{(k+1)} - s^{(k)}\right] + \left[s^{(k+1)} - s^{(k)}\right]\mathfrak{A}^{(k)}\\ &\quad + \mathfrak{A}^{(k-1)^T}\left[s^{(k+1)} - s^{(k)}\right] + s^{(k)}\left[\mathfrak{A}^{(k)} - \mathfrak{A}^{(k-1)}\right]\\ &\quad + \left[\mathfrak{A}^{(k)} - \mathfrak{A}^{(k-1)}\right]^T s^{(k+1)} + \mathfrak{Q}^{(k)} - \mathfrak{Q}^{(k-1)} = 0\end{aligned} \tag{43}$$

where

$$\mathfrak{A}^{(k)} = A - B^{(k)} R^{-1} \left(B^{(k)}\right)^T s^{(k+1)} \tag{44}$$

$$\mathfrak{Q}^{(k)} = \Omega + s^{(k+1)} B^{(k)} R^{-1} \left(B^{(k)}\right)^T s^{(k+1)}. \tag{45}$$

In order to express the solutions of (42) and (43), we introduce the transition matrix $\Phi^{(k)}(t, t_0)$

$$\dot{\Phi}^{(k+1)}(t, t_0) = \mathfrak{A}^{(k)}(t)\Phi^{(k+1)}(t, t_0), \quad \Phi^{(k+1)}(t_0, t_0) = I. \tag{46}$$

In the subsequent proof we will use some of the following properties of the transition matrix $\Phi(\cdot, \cdot)$:

$$\Phi(t, \tau)\Phi(\tau, t_0) = \Phi(t, t_0), \quad \Phi^{-1}(t, \tau) = \Phi(\tau, t). \tag{47}$$

Lemma 1: The solutions of (42) and (43) are

$$\mathrm{e}^{(k+1)} - \mathrm{e}^{(k)} = \int_{t_0}^{t} \Phi^{(k+1)}(t, \tau) \times \left(\mathfrak{A}^{(k)}(\tau) - \mathfrak{A}^{(k-1)}(\tau)\right) \times \Phi^{(k)}(\tau, t_0)\mathrm{e}^0 d\tau \tag{48}$$

and

$$\begin{aligned} & s^{(k+1)} - s^{(k)} \\ &= \int_t^{t_f} [\Phi^{(k)}(\tau, t)]^T \\ &\times \left\{ s^{(k)} \left[\mathfrak{A}^{(k)} - \mathfrak{A}^{(k-1)}\right] + \left[\mathfrak{A}^{(k)} - \mathfrak{A}^{(k-1)}\right]^T s^{(k+1)} \right. \\ &\qquad \left. + \mathfrak{Q}^{(k)} - \mathfrak{Q}^{(k-1)} \right\} \Phi^{(k+1)}(\tau, t) d\tau. \end{aligned} \tag{49}$$

Proof: The integral expression for $\mathrm{e}^{(k+1)} - \mathrm{e}^{(k)}$ can be obtained by directly integrating both sides of the linear system (42). This expression is written in terms of the transition matrix $\Phi(t, t_0)$ defined in (46)–(47). We note that the initial value of the difference term $\mathrm{e}^{(k+1)}(t_0) - \mathrm{e}^{(k)}(t_0) = 0$ due to (36). Therefore, only the inhomogeneous term of the solution appears in (48), where we additionally use the transition matrix to write $\mathrm{e}^{(k)}(\tau) = \Phi^{(k)}(\tau, t_0)\mathrm{e}_0$. By using the variation of the constant method for solving differential equations and the definition of the system transition matrix (47), the expression (48) can be easily obtained.

For the integral expression for $s^{(k+1)} - s^{(k)}$, we first use the definition (46)–(47) of the transition matrix to compute the time derivative $(d/dt)\left\{\left[\Phi^{(k)}(t, t_0)\right]^T \left[s^{(k+1)} - s^{(k)}\right] \Phi^{(k+1)}(t, t_0)\right\}$. Then, by taking into account (43), the resulting time derivative expression is integrated on both sides from t to t_f to obtain

$$\begin{aligned} & \left[\Phi^{(k)}(t, t_0)\right]^T \left[s^{(k+1)} - s^{(k)}\right] \Phi^{(k+1)}(t, t_0) \\ &= \int_t^{t_f} \left[\Phi^{(k)}(\tau, t_0)\right]^T \left\{ s^{(k)} \left[\mathfrak{A}^{(k)} - \mathfrak{A}^{(k-1)}\right] \right. \\ &\qquad \left. + \left[\mathfrak{A}^{(k)} - \mathfrak{A}^{(k-1)}\right]^T s^{(k+1)} + \mathfrak{Q}^{(k)} - \mathfrak{Q}^{(k-1)} \right\} \\ &\quad \times \Phi^{(k+1)}(\tau, t_0) d\tau \end{aligned} \tag{50}$$

where the final difference term $s^{(k+1)}(t_f) - s^{(k)}(t_f)$ vanishes due to the terminal condition $s^{(k+1)}(t_f) = S$ in (38). In order to cancel $\left[\Phi^{(k)}(t, t_0)\right]^T$ and $\Phi^{(k+1)}(t, t_0)$ in (50), we multiply both sides of the (50) with $\left[\Phi^{(k)}(t_0, t)\right]^T$ (from the left) and $\Phi^{(k+1)}(t_0, t)$ (from the right) respectively, and use (47) to obtain the integral expression for $s^{(k+1)} - s^{(k)}$. ■

Theorem 2: There exists an appropriate control weight matrix R, such that the sequences $\{\mathrm{e}^{(k)}(t)\}$ and $\{s^{(k)}(t)\}$ generated by (38) and (39) are convergent.

Proof: Taking the $\|\cdot\|_{\mathfrak{B}}$—norm of $\mathrm{e}^{(k+1)} - \mathrm{e}^{(k)}$ and $s^{(k)} - s^{(k-1)}$ derived in Lemma 1, we have

$$\left\|\mathrm{e}^{(k+1)} - \mathrm{e}^{(k)}\right\|_{\mathfrak{B}_1} \le \mu_1 \left\|\mathfrak{A}^{(k)} - \mathfrak{A}^{(k-1)}\right\|_{\mathfrak{B}_2} \tag{51}$$

$$\left\|s^{(k+1)} - s^{(k)}\right\|_{\mathfrak{B}_2} \le \mu_2 \left\|\mathfrak{A}^{(k)} - \mathfrak{A}^{(k-1)}\right\|_{\mathfrak{B}_2} + \mu_3 \left\|\mathfrak{Q}^{(k)} - \mathfrak{Q}^{(k-1)}\right\|_{\mathfrak{B}_2} \tag{52}$$

where

$$\begin{aligned} \mu_1 &= \max_{t_0 \le \tau \le t \le t_f} \left\|\Phi^{(k+1)}(t, \tau)\right\| \left\|\Phi^{(k)}(\tau, t_0)\right\| \|\mathrm{e}_0\|, \\ \mu_2 &= \max_{t_0 \le t \le \tau \le t_f} \left\|\Phi^{(k)}(\tau, t)\right\| \left(\|s^{(k+1)}\| + \|s^{(k)}\|\right) \\ &\quad \times \left\|\Phi^{(k+1)}(\tau, t)\right\|, \\ \mu_3 &= \max_{t_0 \le t \le \tau \le t_f} \left\|\Phi^{(k)}(\tau, t)\right\| \left\|\Phi^{(k+1)}(\tau, t)\right\|. \end{aligned}$$

By noting (44) and (45), and by defining $\mathcal{S}^{(k)} \triangleq B^{(k)} R^{-1} B^{(k)^T}$, we obtain the following norm bounds:

$$\begin{aligned} & \left\|\mathfrak{A}^{(k)} - \mathfrak{A}^{(k-1)}\right\|_{\mathfrak{B}_2} \\ &= \left\|\mathcal{S}^{(k)} s^{(k+1)} - \mathcal{S}^{(k-1)} s^{(k)}\right\|_{\mathfrak{B}_2} \\ &\le \left\|\left(\mathcal{S}^{(k)} - \mathcal{S}^{(k-1)}\right) s^{(k+1)}\right\|_{\mathfrak{B}_2} \\ &\quad + \left\|\mathcal{S}^{(k-1)} \left(s^{(k+1)} - s^{(k)}\right)\right\|_{\mathfrak{B}_2} \end{aligned} \tag{53}$$

$$\begin{aligned} & \left\|\mathfrak{Q}^{(k)} - \mathfrak{Q}^{(k-1)}\right\|_{\mathfrak{B}_2} \\ &\le \left\|s^{(k+1)} - s^{(k)}\right\|_{\mathfrak{B}_2} \left\|\mathcal{S}^{(k)} s^{(k+1)}\right\|_{\mathfrak{B}_2} \\ &\quad + \left\|s^{(k)}\right\|_{\mathfrak{B}_2} \left\|\mathcal{S}^{(k)} - \mathcal{S}^{(k-1)}\right\|_{\mathfrak{B}_2} \left\|s^{(k)}\right\|_{\mathfrak{B}_2} \\ &\quad + \left\|s^{(k)} \mathcal{S}^{(k)}\right\|_{\mathfrak{B}_2} \left\|s^{(k+1)} - s^{(k)}\right\|_{\mathfrak{B}_2}. \end{aligned} \tag{54}$$

Now we connect the terms in (53) and (54) with the factors $\left\|\mathrm{e}^{(k+1)} - \mathrm{e}^{(k)}\right\|_{\mathfrak{B}_2}$ and $\left\|s^{(k+1)} - s^{(k)}\right\|_{\mathfrak{B}_2}$ to obtain

$$\begin{aligned} & \left\|\mathcal{S}^{(k)} - \mathcal{S}^{(k-1)}\right\|_{\mathfrak{B}_2} \\ &\le \left\|B^{(k)} - B^{(k-1)}\right\|_{\mathfrak{B}_2} \left\|R^{-1} B^{(k)^T}\right\|_{\mathfrak{B}_2} \\ &\quad + \left\|B^{(k-1)} R^{-1}\right\|_{\mathfrak{B}_2} \left\|B^{(k)^T} - B^{(k-1)^T}\right\|_{\mathfrak{B}_2} \\ &\le \frac{\left(\left\|B^{(k)^T}\right\|_{\mathfrak{B}_2} + \left\|B^{(k-1)}\right\|_{\mathfrak{B}_2}\right) \|\Gamma\|_{\mathfrak{B}_2}}{\|R\|} \\ &\quad \times \left\|\mathrm{e}^{(k)} - \mathrm{e}^{(k-1)}\right\|_{\mathfrak{B}_2}. \end{aligned} \tag{55}$$

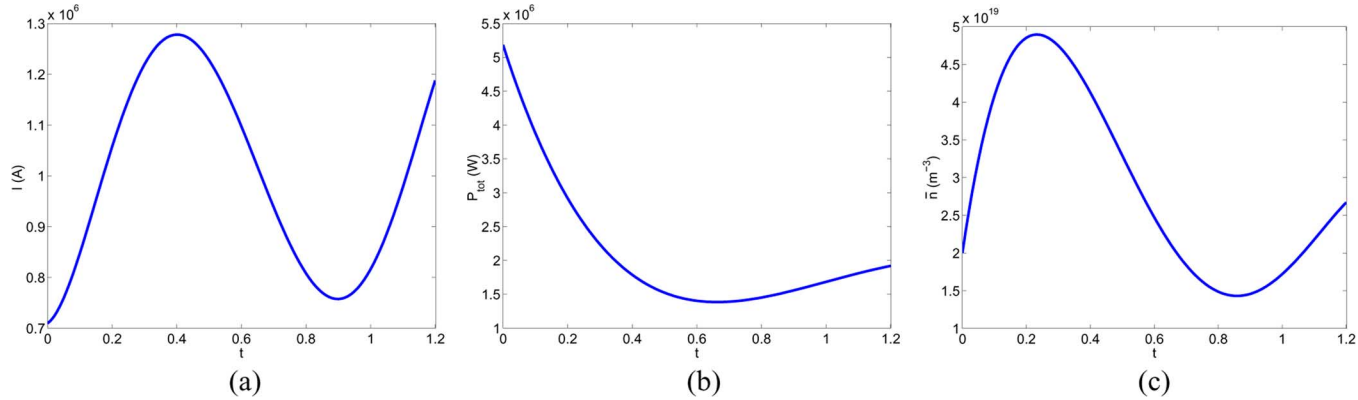

Fig. 3. Open-loop optimal control trajectories: (a) $I(t)$, (b) $P_{\rm tot}(t)$, (c) $\bar{n}(t)$.

Using the norm bound estimates in (51)–(55), we obtain

$$\left\|\mathrm{e}^{(k+1)}-\mathrm{e}^{(k)}\right\|_{\mathfrak{B}_1}\le\nu_1\left\|s^{(k+1)}-s^{(k)}\right\|_{\mathfrak{B}_2}+\nu_2\left\|\mathrm{e}^{(k)}-\mathrm{e}^{(k-1)}\right\|_{\mathfrak{B}_2} \tag{56}$$

where ν_1 and ν_2 are defined as

$$\nu_1=\mu_1\left\|\mathcal{S}^{(k-1)}\right\|_{B_2}$$
$$\nu_2=\mu_1\|s^{(k+1)}\|_{B_2}\frac{\left(\left\|B^{(k)^T}\right\|_{B_2}+\left\|B^{(k-1)}\right\|_{\mathfrak{B}_2}\right)\|\Gamma\|_{\mathfrak{B}_2}}{\|R\|} \tag{57}$$

and

$$\left\|s^{(k+1)}-s^{(k)}\right\|_{\mathfrak{B}_2}\le\nu_3\left\|s^{(k+1)}-s^{(k)}\right\|_{\mathfrak{B}_2}+\nu_4\left\|\mathrm{e}^{(k)}-\mathrm{e}^{(k-1)}\right\|_{\mathfrak{B}_2} \tag{58}$$

where

$$\nu_3=\mu_2\left\|\mathcal{S}^{(k-1)}\right\|_{\mathfrak{B}_2}\mu_3\left\|\mathcal{S}^{(k)}\right\|_{\mathfrak{B}_2}\times\left(\left\|s^{(k)}\right\|_{\mathfrak{B}_2}+\left\|s^{(k+1)}\right\|_{\mathfrak{B}_2}\right)$$
$$\nu_4=\frac{\mu_2\nu_2}{\mu_1}+\frac{\mu_3\nu_2}{\mu_1}\frac{\left\|s^{(k)}\right\|^2_{\mathfrak{B}_2}}{\left\|s^{(k+1)}\right\|_{\mathfrak{B}_2}}. \tag{59}$$

We note that (58) can be solved with respect to $\left\|s^{(k+1)}-s^{(k)}\right\|_{\mathfrak{B}_2}$, i.e.,

$$\left\|s^{(k+1)}-s^{(k)}\right\|_{\mathfrak{B}_2}\le\frac{\nu_4}{1-\nu_3}\left\|\mathrm{e}^{(k)}-\mathrm{e}^{(k-1)}\right\|_{\mathfrak{B}_1}. \tag{60}$$

By substituting (60) into (56), we obtain

$$\left\|\mathrm{e}^{(k+1)}-\mathrm{e}^{(k)}\right\|_{\mathfrak{B}_1}\le\frac{\nu_2+\nu_4(\nu_1-\nu_2)}{1-\nu_4}\left\|\mathrm{e}^{(k)}-\mathrm{e}^{(k-1)}\right\|_{\mathfrak{B}_1}.$$

At this point, it is important to mention that because of the multiplicative influence of R^{-1} in (57) and (59) for ν_2 and ν_4, respectively, if $\|R\|$ is large enough, we can make sure that the coefficients involved are less than one, i.e., $\max\{|\nu_4/1-\nu_3|,|\nu_2+\nu_4(\nu_1-\nu_2)/1-\nu_4|\}<1$. Thus, we can conclude that both $\{s^{(k)}\}$ and $\{\mathrm{e}^{(k)}\}$ are Cauchy sequences

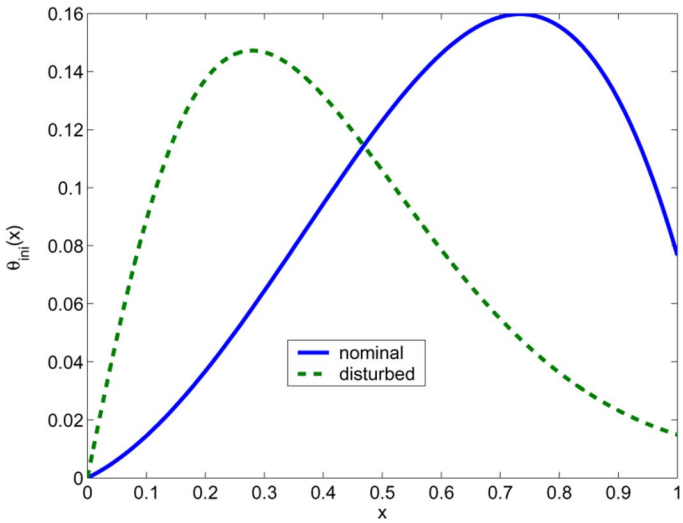

Fig. 4. Comparison of initial θ profiles.

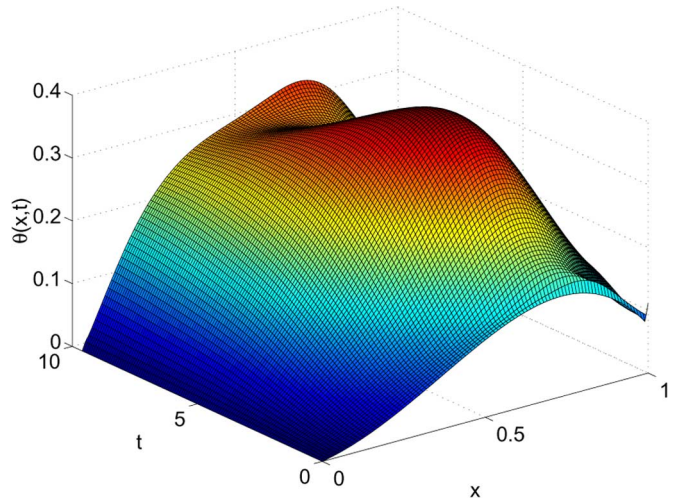

Fig. 5. Time evolution of the θ profile predicted by the original PDE model.

in the associated Banach spaces, i.e., $\left\|s^{(k+1)}-s^{(k)}\right\|_{\mathfrak{B}_2}\to 0$, $\left\|\mathrm{e}^{(k+1)}-\mathrm{e}^{(k)}\right\|_{\mathfrak{B}_1}\to 0$. Due to the completeness of the Banach space, any Cauchy sequence in such a complete space is convergent, thus

$$\lim_{k\to\infty}s^{(k)}(t)=s^*(t),\quad\lim_{k\to\infty}\mathrm{e}^{(k)}(t)=\mathrm{e}^*(t). \tag{61}$$

■

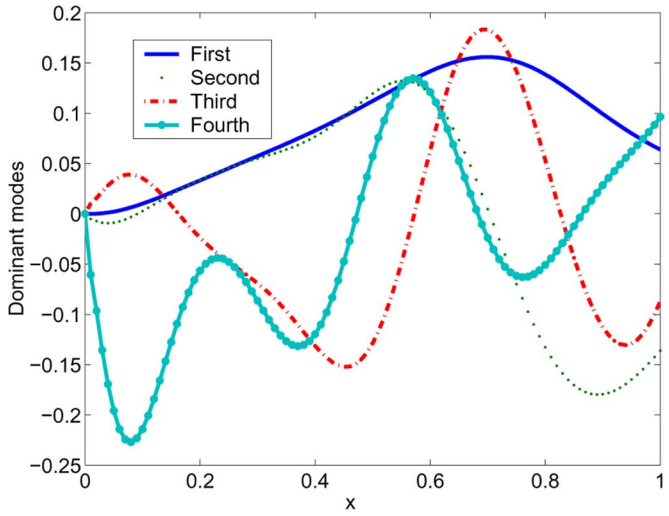

Fig. 6. First four more energetic POD modes.

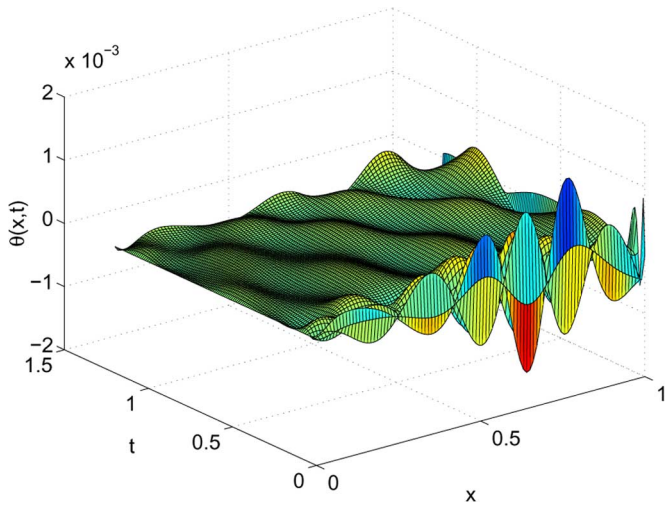

Fig. 7. Time evolution difference for the θ profiles predicted by the original PDE and reduced ODE models.

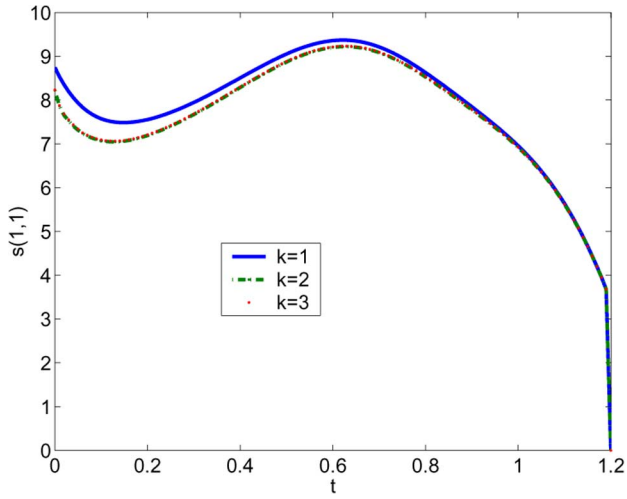

Fig. 8. Convergence of the first diagonal element of s.

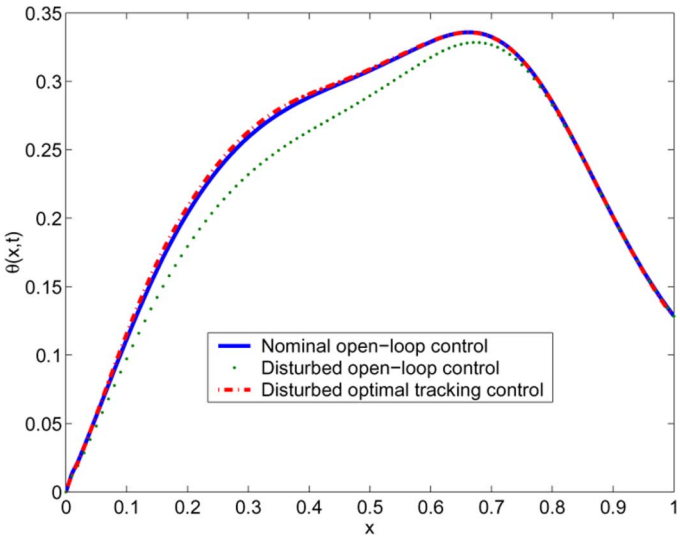

Fig. 9. Final time θ matching comparison.

VI. Simulation Study

We present simulation results showing the effectiveness of the proposed optimal control algorithm in a disturbance rejection problem. For this simulation study we consider a time interval $[t_0 = 0, t_f = T = 1.2s]$ relative to an initial time $t_{\text{ini}} = 500$ ms in the experiment, i.e., $t_0 = 0$ in the simulations corresponds to $t_{\text{ini}} = 500$ ms in the experiment. Fig. 3 shows the time evolutions for $I(t)$, $P_{\text{tot}}(t)$ and $\bar{n}(t)$ obtained from an extremum-seeking offline optimization procedure [6] and from which the control inputs $v^o(t)$ are computed according to (5) and (21). The synthesis of this open-loop optimal controller considered the nominal initial profile $\theta_{\text{ini}}(x)$ shown in Fig. 4, which has been extracted from DIII-D physical shot 129400 at $t_{\text{ini}} = 500$ ms. Fig. 5 illustrates the space-time evolution of $\theta(t,x)$ as predicted by the original PDE system (8) for the nominal initial profile $\theta_{\text{ini}}(x)$ shown in Fig. 4 and the extremum-seeking-based open-loop control $v^o(t)$ shown in Fig. 3. By simulating the original PDE system (8), a data ensemble is created with snapshots of the $\theta(t,x)$ space-time evolution. POD modes are then extracted from the created data ensemble. A total of eight POD modes is considered for model reduction (the first four dominant POD modes are shown in Fig. 6). With these eight POD modes, a low dimensional dynamical system, governed by the ordinary differential equation (ODE) system (22), is obtained. Before computing the closed loop control based on the reduced-order model, we assess the effectiveness of the reduced-order model in approximating the original PDE system. Fig. 7 shows the approximation error as function of time and space. By comparing the magnitude orders in Figs. 5 and 7 we can note that the approximation error is less than 1%. The order of the error demonstrate that the reduced-order model based on only eight POD modes can successfully approximate the PDE system.

The first four more energetic POD modes.

For the functional (26), we choose $R = \text{diag}\left\{\left(200/\max\left(v_1^{ol}\right)\right), \left(2/\max\left(v_2^{ol}\right)\right), \left(200/\max\left(v_3^{ol}\right)\right)\right\}$, $\Omega = \text{diag}\{100, 100, 10, 1, 1, 1, 1, 1, \}$, $S = \text{diag}\{20, 5, 0.1, 0.10.1, 0.10.1, 0.10.1, 0.1\}$, where $\max(v_i^o)$ stands for the maximum value of the open-loop control $v_i^o(t)$. We use the proposed iterative quasi-linear approximation scheme to compute the optimal control law. After iteration $k = 3$,

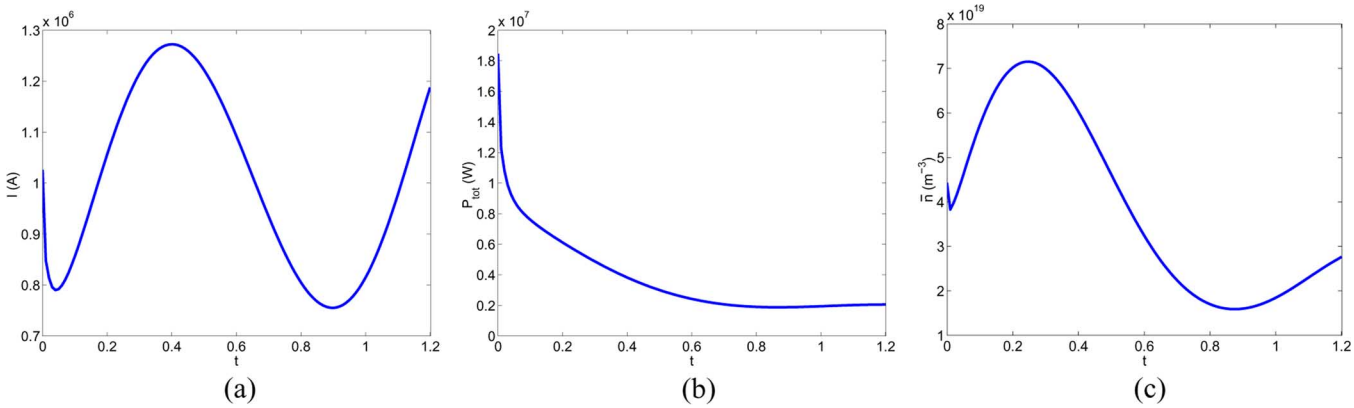

Fig. 10. Optimal tracking control trajectories: (a) $I(t)$, (b) $P_{\rm tot}(t)$, (c) $\bar{n}(t)$.

the solution of the Riccati matrix equation converges, and the feedback controller is implemented according to (40). Fig. 8 shows the first diagonal element of s as a function of the iteration number.

We consider now a disturbed initial profile $\theta_{\rm ini}(x)$, as shown in Fig. 4, and compare the performances of both open-loop and closed-loop controllers in the presence of this disturbance. Fig. 9 shows the difference between the final-time profiles $\theta(x,t_f)$ obtained with the open-loop and closed-loop controllers. The solid blue line shows the final profile obtained with the open-loop controller when there is no disturbance in the initial condition. It is possible to note how the closed-loop controller (red dashed-dotted line) recovers the open-loop undisturbed final profile even in the presence of a substantial disturbance in the initial profile. It is also possible to note how the disturbance in the initial profile is propagated to the final profile in the open-loop control case (green dotted line). In the case of the open-loop controller, the control input trajectories shown in Fig. 3, and computed for the nominal initial profile, are used. In the case of the closed-loop controller, the control input trajectories are shown in Fig. 10.

VII. Conclusion and Future Work

In this paper, we consider a simplified dynamic model describing the evolution of the poloidal flux during the inductive phase of the tokamak discharge. The evolution in time of the current profile is related to the evolution of the poloidal flux, which is modeled in normalized cylindrical coordinates using a PDE usually referred to as the magnetic diffusion equation. An optimal tracking control problem is defined around a nominal open-loop trajectory to overcome uncertainties in the initial conditions. Diffusivity, interior, and boundary actuation is considered for the solution of this optimal control problem.

The control approach is based on model reduction via POD and Galerkin projection methods. A conventional integration-by-parts approach during the Galerkin projection fails to effectively incorporate the considered Dirichlet boundary control into the reduced-order model. To overcome this limitation we use a spatial discretization of the interior product during the Galerkin projection. The obtained low dimensional dynamical model is bilinear as the result of the presence of the diffusivity control term in the parabolic PDE system.

We propose a convergent successive scheme based on the quasi-linearization of the system dynamics to compute an optimal tracking control law for the bilinear reduced-order system. Convergence of the iterative scheme is proved in appropriate functional spaces by exploiting the contraction mapping theorem. The simulation study shows that the proposed controller can effectively overcome the effect of disturbances in the initial poloidal flux profile.

The experimental validation of this control law at the DIII-D tokamak is part of our future work. The current profile controller will have a feedforward component obtained via offline open-loop control design based on highly complex predictive codes and a feedback component designed as proposed in this work based on simplified control-oriented models.

References

[1] A. Pironti and M. Walker, "Fusion, tokamaks, and plasma control," *IEEE Control Syst. Mag.*, vol. 25, no. 5, pp. 30–43, Sep. 2005.

[2] J. P. Freidberg, *Ideal Magnetohydrodynamics*. New York: Plenum Press, 1987.

[3] E. Witrant *et al.*, "A control-oriented model of the current profile in tokamak plasma," *Plasma Phys. Control. Fusion*, vol. 49, pp. 1075–1105, 2007.

[4] Y. Ou, E. Schuster, T. Luce, J. Ferron, M. Walker, and D. Humphreys, "Towards model-based current profile control at DIII-D," *Fusion Eng. Des.*, vol. 82, pp. 1153–1160, 2006.

[5] M. Murakami, , M.R. Wade, C. M. Greenfield, T. C. Luce, J. R. Ferron, H. E. S. John, J. C. DeBoo, W. W. Heidbrink, Y. Luo, and M. A. Makowski, "Progress toward fully noninductive, high beta conditions in DIII-D," *Phys. Plasmas*, vol. 13, no. 5, pp. 056106–056106, 2006.

[6] Y. Ou, C. Xu, E. Schuster, T. Luce, J. Ferron, M. Walker, and D. Humphreys, "Design and simulation of extremum-seeking open-loop optimal control of current profile in the DIII-D tokamak," *Plasma Phys. Controlled Fusion*, vol. 50, pp. 115001–115001, 2008.

[7] C. Xu, J. Dalessio, Y. Ou, E. Schuster, T. Luce, J. Ferron, M. Walker, and D. Humphreys, "Ramp-up phase current profile control of tokamak plasmas via nonlinear programming," *IEEE Trans. Plasma Sci.*, vol. 38, no. 2, pp. 163–173, Feb. 2010.

[8] P. Holmes, J. Lumley, and G. Berkooz, *Turbulence, Coherent Structures, Dynamical Systems and Symmetry*. New York: Cambridge University Press, 1996.

[9] K. Kunisch and S. Volkwein, "Galerkin proper orthogonal decomposition methods for parabolic problems," *Numerische Mathematik*, vol. 90, pp. 117–148, 2001.

[10] E. P. Hofer and B. Tibken, "An iterative method for the finite-time bilinear-quadratic control problem," *J. Optimization Theory Appl.*, vol. 57, pp. 411–427, 1988.

[11] A. Bensoussan, G. D. Prato, M. C. Delfour, and S. K. Mitterl, *Representation and Control of Infinite Dimensional Sysetms*. New York: Springer, 2006.

[12] K. Kunisch and B. Vexler, "Constrained Dirichlet boundary control in L_2 for a class of evolution equations," *SIAM J. Control Opt.*, vol. 46, no. 5, pp. 1726–1753, 2007.

[13] M. Efe and H. Ozbay, "Integral action based Dirichlet boundary control of Burgers equation," in *Proc. IEEE Conf. Control Appl.*, 2003, pp. 1267–1272.